Simple and universal method in designs of high-efficiency diffractive optical elements for spectrum separation and beam concentration*

Wen-Qi Xu(徐文琪)[1], Dong-Feng Lin(林冬风)[2], Xin Xu(许信)[2], Jia-Sheng Ye(叶佳声)[1,†], Xin-Ke Wang(王新柯)[1], Sheng-Fei Feng(冯胜飞)[1], Wen-Feng Sun(孙文峰)[1], Peng Han(韩鹏)[1], Yan Zhang(张岩)[1], Qing-Bo Meng(孟庆波)[2], and Guo-Zhen Yang(杨国桢)[2]

[1] *Department of Physics, Capital Normal University, Beijing Key Laboratory of Metamaterials and Devices, Key Laboratory of Terahertz Optoelectronics of Ministry of Education, Beijing* 100048, *China*
[2] *Institute of Physics, Chinese Academy of Sciences, Beijing* 100190, *China*

(Received 9 January 2017; revised manuscript received 5 March 2017; published online 6 June 2017)

Diffractive optical elements (DOEs) with spectrum separation and beam concentration (SSBC) functions have important applications in solar cell systems. With the SSBC DOEs, the sunlight radiation is divided into several wave bands so as to be effectively absorbed by photovoltaic materials with different band gaps. A new method is proposed for designing high-efficiency SSBC DOEs, which is physically simple, numerically fast, and universally applicable. The SSBC DOEs are designed by the new design method, and their performances are analyzed by the Fresnel diffraction integral method. The new design method takes two advantages over the previous design method. Firstly, the optical focusing efficiency is heightened by up to 10%. Secondly, focal positions of all the designed wavelengths can be designated arbitrarily and independently. It is believed that the designed SSBC DOEs should have practical applications to solar cell systems.

Keywords: diffractive optical element, spectrum separation and beam concentration, optical focusing efficiency, solar cell system

PACS: 42.15.Eq, 42.25.Fx, 42.79.Ek **DOI:** 10.1088/1674-1056/26/7/074202

1. Introduction

Nowadays, environment pollution and energy shortage have become serious problems for sustainable development of society. Solar energy, as a clear, abundant, and renewable energy, is intensively investigated. Solar energy is utilized through converting the photon energy into electricity by the photovoltaic (PV) effect, where the conversion efficiency is the key issue for its wide utilization. If the photon energy is greater than the PV material band gap, the band-gap energy will be absorbed by the solar cell and transferred into electricity, while the excess energy will be transferred into heat.[1] Because the solar radiation is a wideband light source, the efficiency of a single junction solar cell is limited. According to Schockley–Queisser equation,[2] the theoretical conversion efficiency is less than 33% for a single junction silicon solar cell. To improve the conversion efficiency, multi-junction solar cells are necessary so that the incident sunlight within different wave bands is absorbed effectively by different PV materials with the corresponding band gaps.

Generally, there are two ways for multi-junction solar cells. In one way, various semiconductor layers with different band gaps are stacked in series from top to bottom, which are called as tandem multi-junction cells. In the tandem multi-junction cells, each layer absorbs the corresponding waveband of solar radiation and therefore the total conversion efficiency is much higher than the conversion efficiency of the single junction solar cell.[3,4] However, this design encounters two problems of lattice matching and current matching,[4–6] which significantly heighten the fabrication cost and difficulty. An alternative way called parallel multi-junction solar cells is proposed, in which the vertical tandem structure is changed into a transverse parallel structure.[7–10] In the parallel multi junction solar cells, the sunlight is spectrally separated and directed to different PV materials by a spectrum separation optical element. Therefore, we can simplify the cell fabrication as well as circuit connections. Such spectrum separation optical elements mainly include prism,[10] thin-film wave interference filters,[11–15] rugate filters,[16] and diffractive optical elements (DOEs).[17–27] Very recently, Luo *et al.* developed broadband holograms for orbital angular momentum control[28] or 3D display[29] based on electromagnetic resonance at metasurfaces.[30] This kind of metasurface-based devices shows potential applications for spectrum separation in solar cells, on furthering heightening its conversion efficiency.

Besides spectrum separation, beam concentration of the sunlight is also desired since the expensive solar cell materials can be reduced to lower the cell cost. Among the above-

*Project supported by the National Basic Research Program of China (Grant No. 2013CBA01702), the National Natural Science Foundation of China (Grant Nos. 11474206, 91233202, 11374216, and 11404224), the Scientific Research Project of Beijing Education Commission, China (Grant No. KM201310028005), and the Scientific Research Base Development Program of the Beijing Municipal Commission of Education and the Beijing Youth Top-Notch Talent Training Plan, China (Grant No. CIT&TCD201504080).

†Corresponding author. E-mail: jsye@mail.cnu.edu.cn

© 2017 Chinese Physical Society and IOP Publishing Ltd

mentioned spectrum separation optical elements, the DOE is superior in that it integrates both spectrum separation and beam concentration (SSBC) functions due to its micro-sized structures, while the others can only implement the spectrum separation function.[10–13] Consequently, the DOE decreases the optical losses at multiple interfaces, eliminates the alignment error, and enhances the system stability. In some other literature, Castro *et al.* reported that the DOE also helps to relieve the dependence on the illumination angle,[31] and they achieved nearly 50% optical efficiency without the solar tracking system. In previous papers, scientists designed the DOEs by various methods, aiming at different applications. Stefancich *et al.*[17,18] and Michel *et al.*[19,20] designed the SSBC DOEs by the ray tracing method for photovoltaic (PV) systems, but the designed DOEs were too thick (hundreds of micrometers) for photolithographic fabrications. Menon *et al.* applied the extended direct binary search algorithm to designs of the SSBC DOEs[21,22] and a 20% increase in the total electric power was experimentally demonstrated, in comparison with the same cells without the DOEs.[23] Xiao *et al.*[24] designed a DOE by the inversely electromagnetic optimization method, and the spectrum separation efficiency achieved 80.4%. Dong *et al.* designed the SSBC DOEs by an iterative method for optical interconnection systems,[25–27] where the optical focusing efficiencies were below 20%, too low for solar cell applications. The reason is that a phase larger than 2π cannot be extracted by the iterative method. Breaking the 2π phase confinement is indispensable to heighten the focusing efficiency of the designed SSBC DOE. Vorndran *et al.* developed an iterative method for designing broadband DOEs with phase larger than 2π and obtained a high optical efficiency.[32]

Recently, we developed a thickness optimization algorithm for designs of the SSBC DOEs,[33] in which the DOE thickness was broadened to an arbitrary range according to the fabrication requirements. Consequently, the focusing efficiencies of the designed continuous SSBC DOEs were significantly increased to be higher than 80%. For the 32-level SSBC DOE, the theoretical and experimental focusing efficiencies are 68.07% and 52.9%, respectively.[34] The designing process of the SSBC DOEs in Ref. [33] consists of two steps. In the first step, we calculate the initial thickness for each designed wavelength. For realizing the beam concentration function, the Fresnel lens is designed independently for each designed wavelength. For implementing the spectrum splitting function, we use a common blazed grating for all the designed wavelengths. The initial thickness for a specific wavelength is calculated as the thickness summarization of the corresponding Fresnel lens and the common blazed grating. In the second step, the above-obtained initial thicknesses are synthesized to a unique DOE thickness by the thickness optimization algorithm, and the detailed synthesization process was described in detail in Ref. [33]. Since we used a common blazed grating for all the designed wavelengths in Ref. [33], their preset focal positions could not be altered independently. In addition, the blazed grating is blazing only for a specific wavelength, which decreases the diffraction efficiencies for the other designed wavelengths.

Based on the above two considerations, in the new design method we make an improvement to the blazed grating. In this paper, the blazed grating is designed independently for each designed wavelength, which improves two aspects. On one hand, the preset focal positions can be designated independently since we may arbitrarily select the blazing angle for each designed wavelength. On the other hand, because all the blazed gratings are blazing for the designed wavelengths, the synthesized DOE should have a higher optical focusing efficiency. The new design method is not only physically simple, but also applicably universal. Moreover, by this new design method, a very high optical focusing efficiency of the SSBC DOE can be expected.

This paper is organized as follows. In Section 2, we describe the principles of the new design method with formulas. In Section 3, focal performances of the SSBC DOEs designed by the new method are investigated in detail. In addition, focal performances of the SSBC DOEs designed by the previous method are also presented for comparison. A brief conclusion is drawn in Section 4 with some discussion.

2. Design method of the SSBC DOE

Figure 1 depicts a diffractive geometry of the SSBC DOE, which separates different incident colors and focuses them on different focal positions in the output plane. In solar cell systems, different semiconductors with corresponding band gaps are placed at the focal positions for high-efficient absorption. Next, we will describe the designing process of the SSBC DOE by the new design method, in which the blazed gratings are designed independently for each designed wavelength. Figure 2 depicts the schematic diagram of a bulk SSBC DOE, which is composed of a refractive lens and a prism. The refractive lens implements the beam concentration function. The prism produces an extra oblique phase, leading to a focal point deviation along the transverse direction. The transverse focal position is determined by the apex angle of the prism. In Fig. 2, the apex angles are chosen as different values for different designed wavelengths. Therefore, different colors are separated at different focal positions. Especially, when the apex angle is 0° for wavelength λ_2 (namely, without the prism), the preset focal position is located at the origin point. The thickness function of the refractive lens is given by $h_{\mathrm{rl}}(x,\lambda_i) = -x^2/\{2[n(\lambda_i)-1]f\}$, where $n(\lambda_i)$ represents the material refractive index at wavelength λ_i $(i = 1,2,3,\ldots)$; x

denotes the transverse coordinate in the input plane; f represents the focal distance. The thickness function of the prism is given by $h_{\rm p}(x,\lambda_i) = \tan[\beta(\lambda_i)]x$. Consequently, the thickness of the bulk SSBC DOE for each designed wavelength λ_i is $h_{\rm b}(x,\lambda_i) = h_{\rm rl}(x,\lambda_i) + h_{\rm p}(x,\lambda_i)$. Under normal incidence of a plane wave, the transverse focal position of the above bulk SSBC DOE is deduced from geometrical optics as

$$x_i(\lambda_i) = f \times \tan\{\arcsin\{n(\lambda_i) \times \sin[\beta(\lambda_i)]\} - \beta(\lambda_i)\}. \quad (1)$$

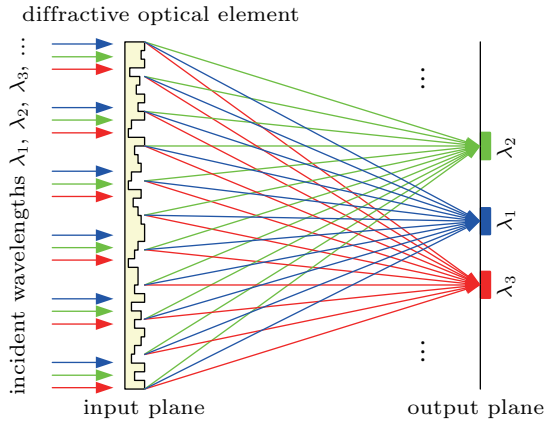


Fig. 1. (color online) A schematic diagram of the diffractive optical element (DOE) for implementing the spectrum separation and beam concentration (SSBC) functions.

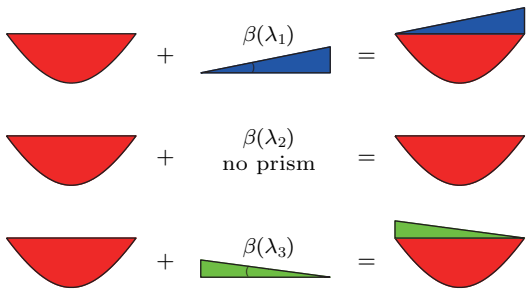


Fig. 2. (color online) A schematic diagram for designing a bulk SSBC DOE, which consists of a refractive lens and a prism.

In physical optics, a 2π phase may be added or removed without influencing the DOE performance. Hence, the refractive lens and the prism can be thinned to a Fresnel lens and a blazed grating, respectively, as shown in Fig. 3. The thickness function of the Fresnel lens is written as $h_{\rm Fl}(x,\lambda_i) = {\rm Mod}[h_{\rm rl}(x,\lambda_i), \Delta h_i]$, where $\Delta h_i = \lambda_i/[n(\lambda_i)-1]$ corresponds to 2π phase modulation for the designed wavelength λ_i; ${\rm Mod}[A,B]$ represents the modulus function and its value ranges from 0 to B. By analogy, the thickness of the blazed grating is $h_{\rm g}(x,\lambda_i) = {\rm Mod}[h_{\rm p}(x,\lambda_i), \Delta h_i]$. Apparently, if we combine the Fresnel lens and the blazed grating together, the combined SSBC DOE will be thinner than $2\Delta h_i$, as shown in Fig. 3. In the meanwhile, it performs the same optical behavior as the bulk SSBC DOE in Fig. 2. In fact, the thickness of the SSBC DOE can be furtherly decreased as $h_i^0(x,\lambda_i) = {\rm Mod}[h_{\rm Fl}(x,\lambda_i) + h_{\rm g}(x,\lambda_i), \Delta h_i]$, which serves as the ground thickness for the designed wavelength λ_i. Here h_i^0 ranges from 0 to Δh_i.

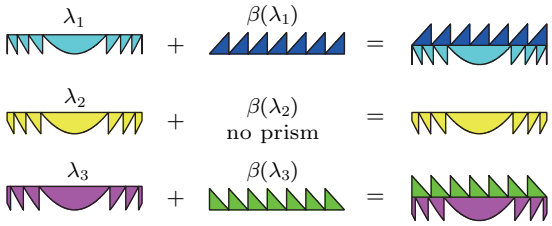


Fig. 3. (color online) A schematic diagram for designing the SSBC DOE, which is composed of a Fresnel lens and a blazed grating.

It is worthy to mention that there exist two essential differences between the new design method and the previous design method in Ref. [33]. In Ref. [33], we used a common blazed grating for all the designed wavelengths (see Fig. 2 of Ref. [33]), which resulted in two consequences. Firstly, the preset focal positions for all the designed wavelengths are correlated with each other. Secondly, the common blazed grating can only have a 100% diffraction efficiency for the blazing wavelength, while for the other designed wavelengths the diffraction efficiencies are somewhat lower. In contrast, in the new design method we make two improvements. Firstly, the apex angle $\beta(\lambda_i)$ is independently chosen for each designed wavelength λ_i. As a result, all the preset focal positions can be designated independently. Secondly, the attenuation from the prism to the blazed grating is handled individually so that the grating diffraction efficiencies are 100% for all the designed wavelengths.

However, the solar cell system works for a broad waveband, rather than a specific wavelength. Generally, we divide the broad waveband into several sub-wavebands. In each subwaveband, we select a design wavelength, corresponding to a definite ground thickness. Then, for such a multiwavelength system, how to synthesize several ground thicknesses to a definite thickness of the SSBC DOE? The thickness synthesization is implemented by the thickness optimization algorithm, whose principle and flow chart were presented in Ref. [33]. Here we just make a brief description.

Let us assume that the maximum designing thickness of the DOE is $h_{\rm max}$, which is usually limited by the experimental fabrication ability. Since multiples of 2π phase do not exert any impact on the DOE's performance, for each designed wavelength there exist a series of alternative thicknesses as follows:

$$h_i = h_i^0 + m\Delta h_i, \quad (2)$$

where h_i^0 is the ground thickness for wavelength λ_i; $m = 0,1,2,\ldots$, and the maximum integer of m is acquired from the inequality $h_i \le h_{\rm max}$; $\Delta h_i = \lambda_i/[n(\lambda_i)-1]$ corresponds to a phase modulation of 2π for wavelength λ_i.

From each set of thicknesses, we arbitrarily select a thickness. If the designing wavelength number is M, we will have M thicknesses altogether. The error between two arbitrary thicknesses is calculated as $\Delta_{ij} = |h_i - h_j|$. We define an error function as

$$\Delta = \sum_{i=1,M}^{j=i+1,M} \Delta_{ij} . \tag{3}$$

The optimal thickness in each set is found through minimizing the error function Δ. Finally, the thickness of the SSBC DOE is averaged as

$$h_{\mathrm{c}} = \frac{1}{M}\sum_{i=1}^{M} h_i . \tag{4}$$

The thickness h_{c} in Eq. (4) may take any continuous value. In photolithography, the DOE is usually fabricated by binary masking technology. If the mask number is K, the quantization level number is $N = 2^K$. When the maximum designing thickness ($h_{\max}$) of the SSBC DOE is equally quantized into N levels, each step depth is $\Delta h = h_{\max}/N$. The thickness of the quantized DOE (h_{q}) is derived from that of the continuous one (h_{c}) as

$$h_{\mathrm{q}} = \mathrm{int}\left(\frac{h_{\mathrm{c}}}{\Delta h}\right) \times \Delta h , \tag{5}$$

where $\mathrm{int}(C)$ means taking the maximum integer no larger than a real number C.

Once the SSBC DOE is designed, the optical field in the input plane is given by

$$U_1(x_1, \lambda_i) = \exp\left\{\mathrm{j}\frac{2\pi[n(\lambda_i) - 1] \times h(x_1)}{\lambda_i}\right\}, \tag{6}$$

where x_1 denotes the transverse coordinate of the sampling point on the input plane; $h(x_1)$ represents the thickness of the DOE; j is the imaginary unit; $h(x_1)$ equals $h_{\mathrm{c}}(x_1)$ or $h_{\mathrm{q}}(x_1)$ for the continuous or quantized SSBC DOE, respectively; $n(\lambda_i)$ stands for material refractive index of DOE. It is noted that the reflection losses on both interfaces of the DOE are ignored. As long as the focal distance is far enough, the Fresnel diffraction integral method is employed to calculate the field in the output plane as[35]

$$U_2(x_2, \lambda_i) = \int U_1(x_1, \lambda_i)\hat{G}(x_2, x_1, \lambda_i)\mathrm{d}x_1 , \tag{7}$$

where x_2 represents the transverse coordinate in the output plane; $\hat{G}$ denotes the Fresnel diffraction integral kernel, as given by

$$\hat{G}(x_2, x_1, \lambda_i) = \frac{1}{\sqrt{\mathrm{j}\lambda_i f}} \exp\left(\mathrm{j}\frac{2\pi f}{\lambda_i}\right) \exp\left[\mathrm{j}\frac{\pi(x_2 - x_1)^2}{\lambda_i f}\right]. \tag{8}$$

In order to characterize the performance of the DOE, the optical focusing efficiency η_i for incident wavelength λ_i is defined as

$$\eta_i = \frac{\int_{x_i - d/2}^{x_i + d/2} |U_2(x_2, \lambda_i)|^2 \mathrm{d}x_2}{\int_{-\infty}^{+\infty} |U_1(x_1, \lambda_i)|^2 \mathrm{d}x_1} , \tag{9}$$

where x_i denotes the geometrical transverse focal position for wavelength λ_i, which can be calculated from Eq. (1); the symbol $|U_j|$ $(j = 1, 2)$ represents the magnitude of a complex number U_j; d represents the integrating width of the focused region. The ultimate optical focusing efficiency of the designed SSBC DOE is averaged as

$$\eta = \frac{1}{M}\sum_{i=1}^{M} \eta_i . \tag{10}$$

3. Focal performances of the SSBC DOEs

To show the validity of our proposed method, designing parameters are selected as follows. We choose three designed wavelengths as $\lambda_1 = 0.45$ μm, $\lambda_2 = 0.55$ μm, and $\lambda_3 = 0.65$ μm. Therefore, the wave number is $M = 3$ in Eq. (10). The central wavelength is $\lambda_0 = 0.55$ μm. The focal distance is $f = 800$ mm. We define a length unit as $l_0 = \sqrt{\lambda_0 \times f} = 0.6633$ mm. The input and output planes have the same sizes of $32l_0 = 21.23$ mm. Both the input and the output planes are equally quantized into 4096 pixels, with the pixel size being 21.23 mm/4096 = 5.18 μm. The grating apex angles are preset to $\beta(\lambda_1) = \pi/880$, $\beta(\lambda_2) = 0$, and $\beta(\lambda_3) = -\pi/880$, respectively. The DOE material is fused silica,[36] whose refractive index varies slightly within the wavelength range [0.45 0.65] μm. In our simulations, the material dispersive effect is ignored and the refractive index of fused silica is computed as $n = 1.46$. For characterizing the optical focusing efficiency, the integrating width of the focused region in Eq. (9) is chosen as $d = 2l_0 = 1.32$ mm.

Firstly, on varying the maximum permitted phase, we design the SSBC DOEs with the above-selected parameters. Figure 4 plots the optical focusing efficiency of the designed SSBC DOEs with respect to the maximum permitted phase. The maximum permitted phase is involved with the central wavelength, namely, an increase of 2π phase leads to a DOE thickness increment of $\Delta h = \lambda_0/(n-1) \approx 1.20$ μm. The blue curve corresponds to the designed SSBC DOEs with continuous phases. In Fig. 4, the optical focusing efficiency of the continuous DOE is monotonically increased as the maximum permitted phase is enlarged, which can be interpreted as follows. On increasing the maximum permitted phase, we have more alternative thicknesses for each designed wavelength. Therefore, the synthesized thickness will be closer to the alternative thickness for each designed wavelength. The maximum optical focusing efficiency reaches as high as 85.94% when the maximum permitted phase is 20π, i.e., the maximum DOE thickness is 12 μm.

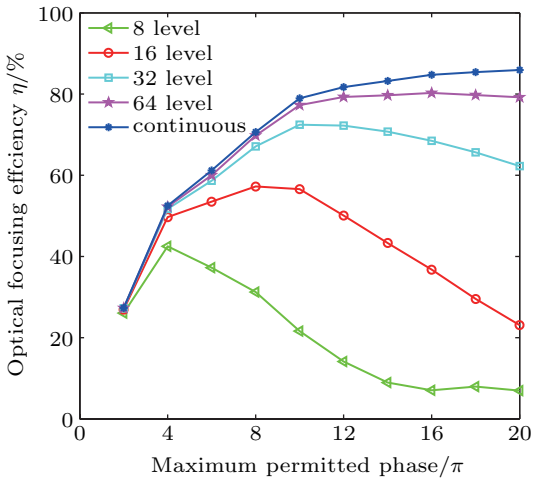


Fig. 4. (color online) Optical focusing efficiency of the designed SSBC DOEs with respect to the maximum permitted phase. The maximum permitted phase is involved with the central wavelength. The green, red, cyan, magenta, and blue curves correspond to the 8-level, 16-level, 32-level, 64-level, and continuous DOEs, respectively.

For practical applications, the designed SSBC DOEs are usually fabricated by binary masking photolithography technology. The above-designed continuous SSBC DOEs needs to be quantized to have a multilevel profile. In Fig. 4, the green, red, cyan, and magenta curves correspond to the 8-level, 16-level, 32-level, and 64-level DOEs, respectively. For a given maximum permitted phase, the optical focusing efficiency is higher when the quantization level number is larger, which is due to the diminishment of the quantization error. For a definite quantization level number, there exists an optimum value for the maximum permitted phase. It can be understood. On one hand, when the maximum permitted phase is too small, the thickness selections are limited and thus the synthesized thickness h_c deviates greatly from the selected thickness h_i for each designed wavelength. On the other hand, when the maximum permitted phase is too large, the boundary quantization error will be increased dramatically as the quantization level number is fixed.

In order to make an equivalent comparison between the new design method and the previous design method in Ref. [33], the choice of the grating apex angle should ensure that the designed incident waves are separated by the same distances for both methods. In Ref. [33], the grating apex angle was selected as $\pi/160$ and the output-plane focal positions are separated by 1.31 mm for the three designed wavelengths. In the present design, from Eq. (1) the grating apex angles should be $\beta(\lambda_1) = \pi/880$, $\beta(\lambda_2) = 0$, and $\beta(\lambda_3) = -\pi/880$. Other parameters are the same as those in Ref. [33]. Figure 5(a) plots the boundary profile of the designed 32-level SSBC DOE, and the inset shows its magnified local part. Figure 5(b) illustrates the output-plane intensity distributions for the three designed wavelengths. It is seen from Fig. 5(b) that the three designed waves are well focused and separated on the output plane. Numerical results reveal that the actual focal positions are 1.31, 0, and −1.31 mm for incident wavelengths of 0.45, 0.55, and 0.65 μm, respectively. The actual focal positions agree with the geometrical focal positions in Eq. (1). The corresponding three optical focusing efficiencies are 63.57%, 73.10%, and 80.08%. Therefore, the average focusing efficiency is 72.25%. In contrast, the average focusing efficiency is 67.75% in Ref. [33]. The efficiency is increased by 4.5%. The efficiency improvement is more prominent when increasing the blazing angle or decreasing the input pixel number. For instance, when the blazing angle is increased from $\pi/880$ to $\pi/660$ and the input pixel number is decreased from 4096 to 2048 with other parameters unchanged, the optical focusing efficiencies of the 32-level DOEs are 67.81% and 57.88% for the new and previous design methods, respectively. The efficiency is heightened by about 10%.

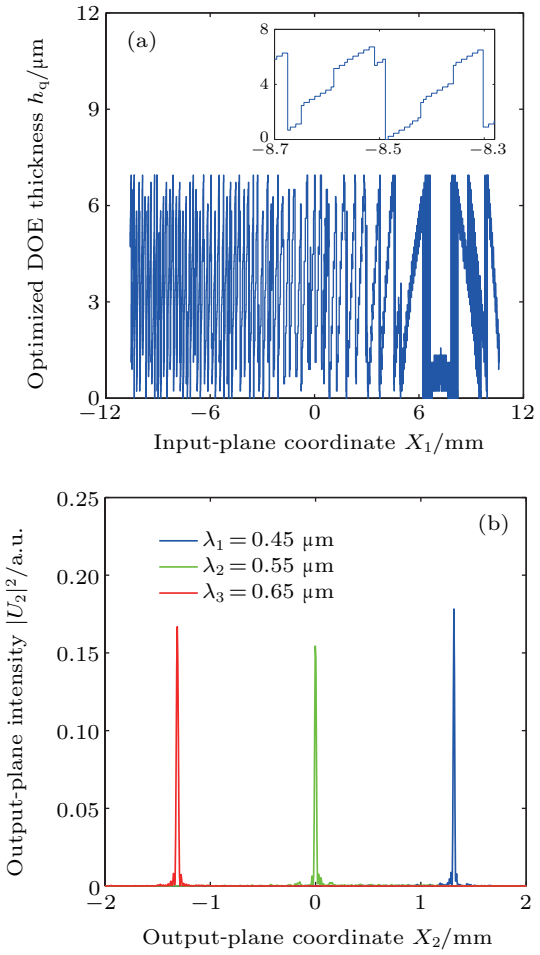


Fig. 5. (color online) (a) Boundary profile of the optimized 32-level SSBC DOE. The inset magnifies the local part of the boundary. (b) Output-plane intensity distributions of the optimized 32-level SSBC DOE with the maximum permitted phase of 12π. The grating apex angles are chosen as $\beta(\lambda_1) = \pi/880$, $\beta(\lambda_2) = 0$, and $\beta(\lambda_3) = -\pi/880$ for incident wavelengths of 0.45, 0.55, and 0.65 μm, respectively. The blue, green, and red curves plot the intensity distributions for incident wavelengths of 0.45, 0.55, and 0.65 μm, respectively.

Although it is shown that the 32-level SSBC DOE has a high efficiency for the three designed wavelengths, its performance for other wavelengths within the considered waveband

is still unclear. Especially, this is critically important for its practical applications to solar cells because the solar radiation has a continuous spectrum. For this purpose, we select 17 incident wavelengths within the waveband [450 650] nm for every 12.5 nm, and calculate the output intensity distributions, as shown in Fig. 6. From Fig. 6, the energy concentration regions are distributed successively, although the intensity peaks for the 14 inserted wavelengths are much lower than those of the three designed wavelengths. In solar cell applications, a regular energy concentration position is more important rather than a high intensity peak, because only under this condition can we align the solar cells with monotonically increasing energy band gaps. Besides the energy concentration position, the other important aspect is the average focusing efficiency in the considered waveband. Numerical results reveal that the average efficiency is 59.25% for the 17 incident wavelengths, when the integrating width is 1.32 mm. Frankly speaking, this is a very conservation estimation. Considering the incident aperture is 21.23 mm, the integrating width may be much larger. If the integrating width is enlarged to 2.64 mm (i.e., 1/8 of the incident aperture), the average efficiency reaches 70.16%. Therefore, it is concluded that the designed 32-level SSBC DOE has a very high efficiency in the considered waveband, ensuring its possible applications in solar cells.

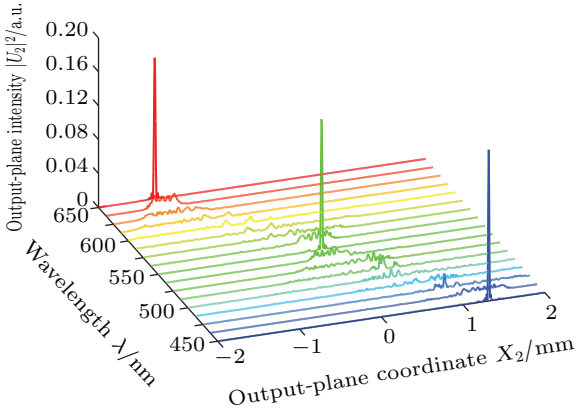


Fig. 6. (color online) Output-plane intensity distributions of the designed 32-level DOE in Fig. 5(a), for the 17 incident wavelengths within the waveband [450 650] nm with an interval of 12.5 nm. The three intensity peaks correspond to the three designed wavelengths of 0.45, 0.55, and 0.65 μm, respectively.

The other advantage of the new design method over the previous design method is that the focal positions can be assigned arbitrarily and independently. Now the grating apex angles are selected as $\beta(\lambda_1) = 0$, $\beta(\lambda_2) = \pi/600$, and $\beta(\lambda_3) = -\pi/500$. Figure 7(a) draws the boundary profile of the designed 32-level SSBC DOE, and the inset shows its magnified local part. Figure 7(b) displays the intensity distributions on the output plane. The blue, green, and red curves correspond to incident wavelengths of 0.45, 0.55, and 0.65 μm, respectively. It is noted that the three waves are no longer aligned in order, and the two separating distances are not equal. Numerical results reveal that the actual focal positions are 0, 1.93, and −2.31 mm for incident wavelengths of 0.45, 0.55, and 0.65 μm, respectively. From Eq. (1), the geometrical focal positions are also 0, 1.93, and −2.31 mm. Optical focusing efficiencies are 60.18%, 62.85%, and 78.25% for incident wavelengths of 0.45, 0.55, and 0.65 μm, respectively. Hence, the average focusing efficiency is 67.09%. Seeing that the integrating width of the focused region is only 1.32 mm (i.e., 1/16 of the incident aperture), this focusing efficiency is still very high.

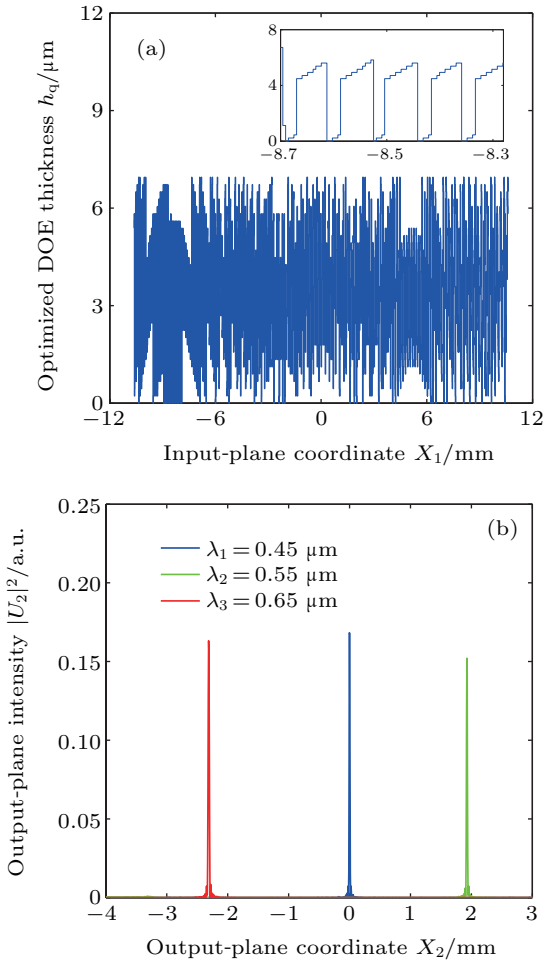


Fig. 7. (color online) (a) Boundary profile of the optimized 32-level SSBC DOE. The inset magnifies the local part of the boundary. (b) Output-plane intensity distributions of the optimized 32-level SSBC DOE with the maximum permitted phase of 12π. The grating apex angles are chosen as $\beta(\lambda_1) = 0$, $\beta(\lambda_2) = \pi/600$, and $\beta(\lambda_3) = -\pi/500$ for incident wavelengths of 0.45, 0.55, and 0.65 μm, respectively. The blue, green, and red curves plot the intensity distributions for incident wavelengths of 0.45, 0.55, and 0.65 μm, respectively.

4. Conclusion and discussion

In summary, we propose a new method for designing SSBC DOEs. The new design method is physically simple, numerically fast, and universally applicable. For the SSBC DOE design in our paper, it costs about one second on a personal computer using 3.0 GHz Core(TM)2 Quad CPU. Nu-

merical examples demonstrate that the designed DOEs have realized the expected SSBC functions with a very high optical focusing efficiency. Compared with previous design method, the new design method has two superiorities. Firstly, the focusing efficiency is increased a lot. Secondly, the focal positions can be designated arbitrarily and independently for all the designed wavelengths, which expands its applications to solar cells with different sizes. For experimental fabrication of the 32-level SSBC DOE in laboratory, we first generate five binary masks. Then, photoresist is spin coated on a fused silica substrate. After micro photolithography, the fused silica substrate is etched with a reactive ion etching machine, followed by a photoresist cleaning process. On repeating the photolithography and etching procedures five times, a final surface-relief structure of the 32-level DOE is formed. For practical applications of the SSBC DOEs to high-efficiency solar cells, massive production is necessary. We can firstly fabricate a mold with complementary structure, and then duplicate the DOEs by the nanoimprint technology, like the fabrication of optical disks.

References

[1] Henry C H 1980 *J. Appl. Phys.* **51** 4494
[2] Shockley W and Queisser H J 1961 *J. Appl. Phys.* **32** 510
[3] Razykov T M, Ferekides C S, Morel D, Stefanakos E, Ullal H S and Upadhyaya H M 2011 *Solar Energy* **85** 1580
[4] Dimroth F, Grave M and Beutel P 2014 *Prog. Photovolt: Res. Appl.* **22** 277
[5] Kurtz S and Geisz J 2010 *Opt. Express* **18** A73
[6] Imenes A G and Mills D R 2004 *Sol. Energy Mater. Sol. Cells* **84** 19
[7] Caselli D, Liu Z C, Shelhammer D and Ning C Z 2014 *Nano Lett.* **14** 5772
[8] Wang J Z, Huang Q L, Xu X, Quan B G, Luo J H, Zhang Y, Ye J S, Li D M, Meng Q B and Yang G Z 2015 *Chin. Phys. B* **24** 054201
[9] Mojiri A, Taylor R, Thomsen E and Rosengarten G 2013 *Renewable & Sustainable Energy Reviews* **28** 654
[10] Barnett A, Kirkpatrick D and Honsberg C 2009 *Prog. Photovolt: Res. Appl.* **17** 75
[11] Green M A, Keevers M J and Thomas I 2015 *Prog. Photovolt: Res. Appl.* **23** 685
[12] Vlasov A S, Khvostikov V P, Karlina L B, Sorokina S V, Potapovich N S, Shvarts M Z, Timoshina N K, Lantratov V M, Mintairov S A, Kalyuzhnyi N A, Marukhina E P and Andreev V M 2013 *Technical. Phys.* **58** 1034
[13] Wang J Z, Ye J S, Huang Q L, Xu X, Li D M, Meng Q B and Yang G Z 2014 *Chin. Phys. B* **23** 044211
[14] Russo J M, Zhang D, Gordon M, Vorndran S, Wu Y C and Kostuk R K 2014 *Opt. Express* **22** A528
[15] Mitchell B, Peharz G, Siefer G, Peters M, Gandy T, Goldschmidt J C, Benick J, Glunz S W, Bett A W and Dimroth F 2011 *Prog. Photovolt: Res. Appl.* **19** 61
[16] Peters M, Goldschmidt J C, Löper P, Groß B, Üpping J, Dimroth F, Wehrspohn R B and Bläsi B 2010 *Energies* **3** 171
[17] Stefancich M, Zayan A, Chiesa M, Rampino S, Roncati D, Kimerling L and Michel J 2012 *Opt. Express* **20** 9004
[18] Maragliano C, Chiesa M and Stefancich M 2015 *J. Opt.* **17** 105901
[19] Michel C, Loicq J, Languy F and Habraken S 2014 *Sol. Energy Mater. Sol. Cells* **120** 183
[20] Michel C, Loicq J, Thibert T and Habraken S 2015 *11th International Conference on Concentrator Photovoltaic Systems, AIP Conf. Proc.* **1679** 070002-1/-7
[21] Kim G, Domínguez-Caballero J A and Menon R 2012 *Opt. Express* **20** 2814
[22] Mohammad N, Wang P, Friedman D J and Menon R 2014 *Opt. Express* **22** A1519
[23] Wang P, Dominguez-Caballero J A, Friedman D J and Menon R 2015 *Prog. Photovolt: Res. Appl.* **23** 1073
[24] Xiao T P, Cifci O S, Bhargava S, Chen H, Gissibl T, Zhou W, Giessen H, Toussaint K C Jr, Yablonovitch E and Braun P V 2016 *ACS Photon.* **3** 886
[25] Dong B Z, Zhang G Q, Yang G Z, Gu B Y, Zheng S H, Li D H, Chen Y S, Cui X M, Chen M L and Liu H D 1996 *Appl. Opt.* **35** 6859
[26] Dong B Z, Yang G Z, Gu B Y and Zhang G Q 1997 *J. Opt. Soc. Am. A* **14** 44
[27] Dong B Z, Liu R, Yang G Z and Gu B Y 1998 *J. Opt. Soc. Am. A* **15** 480
[28] Pu M B, Li X, Ma X L, Wang Y Q, Zhao Z Y, Wang C T, Hu C G, Gao P, Huang C, Ren H R, Li X P, Qin F, Yang J, Gu M, Hong M H and Luo X G 2015 *Sci. Adv.* **1** e1500396
[29] Li X, Chen L W, Li Y, Zhang X H, Pu M B, Zhao Z Y, Ma X L, Wang Y Q, Hong M H and Luo X G 2016 *Sci. Adv.* **2** e1601102
[30] Yu N F, Genevet P, Kats M A, Aieta F, Tetienne J P, Capasso F and Gaburro Z 2011 *Science* **334** 333
[31] Castro J M, Zhang D, Myer B and Kostuk R K 2010 *Appl. Opt.* **49** 858
[32] Vorndran S, Russo J M, Wu Y C, Pelaez S A and Kostuk R K 2015 *Opt. Express* **23** A1512
[33] Ye J S, Wang J Z, Huang Q L, Dong B Z, Zhang Y and Yang G Z 2013 *Chin. Phys. B* **22** 034201
[34] Huang Q L, Wang J, Quan B, Zhang Q L, Zhang D X, Li D M, Meng Q B, Pan L, Wang Y Q and Yang G Z 2013 *Appl. Opt.* **52** 2312
[35] Goodman J W 1968 *Introduction to Fourier Optics* (San Francisco: McGraw-Hill Press) Chaps. 3 and 4
[36] Bass M 1995 *Handbook of Optics, Volumn II, Devices, Measurements, and Properties*, 2nd edn. (NewYork: McGraw-Hill Press) Chap. 33